Analysis of *Escherichia coli* Anaplerotic Metabolism and Its Regulation Mechanisms From the Metabolic Responses to Altered Dilution Rates and Phosphoenolpyruvate Carboxykinase Knockout

Chen Yang,[1] Qiang Hua,[1] Tomoya Baba,[2] Hirotada Mori,[2] Kazuyuki Shimizu[1,3]

[1]Metabolome Unit, Institute for Advanced Biosciences, Keio University, Tsuruoka 997-0017, Japan
[2]Genome Engineering Unit, Institute for Advanced Biosciences, Keio University, Tsuruoka 997-0017, Japan
[3]Department of Biochemical Engineering & Science, Kyushu Institute of Technology, Iizuka 820-8502, Japan; telephone: +81-948-29-7817; fax: +81-948-29-7801; e-mail: shimi@bse.kyutech.ac.jp

Abstract: The gluconeogenic phosphoenolpyruvate (PEP) carboxykinase is active in *Escherichia coli* during its growth on glucose. The present study investigated the influence of growth rates and PEP carboxykinase knockout on the anaplerotic fluxes in *E. coli*. The intracellular fluxes were determined using the complementary methods of flux ratio analysis and metabolic flux analysis based on [U-^{13}C$_6$]glucose labeling experiments and 2D nuclear magnetic resonance (NMR) spectroscopy of cellular amino acids and glycerol. Significant activity of PEP carboxykinase was identified in wild-type *E. coli*, and the ATP dissipation for the futile cycling via this reaction accounted for up to 8.2% of the total energy flux. Flux analysis of *pck* deletion mutant revealed that abolishment of PEP carboxykinase activity resulted in a remarkably reduced flux through the anaplerotic PEP carboxylase and the activation of the glyoxylate shunt, with 23% of isocitrate found being channeled in the glyoxylate shunt. The changes in intracellular metabolite concentrations and specific enzyme activities associated with different growth rates and *pck* deletion, were also determined. Combining the measurement data of in vivo fluxes, metabolite concentrations and enzyme activities, the in vivo regulations of PEP carboxykinase flux, PEP carboxylation, and glyoxylate shunt in *E. coli* are discussed. © 2003 Wiley Periodicals, Inc. *Biotechnol Bioeng* **84**: 129–144, 2003.

Keywords: *Escherichia coli;* metabolic flux; ^{13}C labeling; anaplerotic reaction; phosphoenolpyruvate carboxykinase; in vivo regulation

INTRODUCTION

The central carbon pathways constitute the backbone of cell metabolism by providing cofactors, building blocks, and energy for biomass synthesis. Among the metabolites of the central metabolism, phosphoenolpyruvate (PEP) is an important branch node and plays a key role in the cell physiology. Phosphoenolpyruvate participates in not only the carbohydrate-uptaking phosphotransferase (PTS) system but also the reactions catalyzed by pyruvate kinase and PEP carboxylase. Consequently, the metabolic pathways around the PEP and PYR nodes are often the focus of interest. A number of studies have been focused on understanding and manipulating carbon fluxes around PEP and pyruvate for biotechnological applications (Chao and Liao, 1994; Emmerling et al., 2002; Flores et al., 1996; Petersen et al., 2000).

In *Escherichia coli* the reaction catalyzed by PEP carboxylase is the only anaplerotic reaction converting C$_3$ metabolites to replenish the metabolic pools of the tricarboxylic acid (TCA) cycle. The glyoxylate shunt can also serve an anaplerotic function for the cell growth on acetate, but this pathway is generally considered to be inactive in *E. coli* grown on glucose. In addition, *E. coli* possesses the C$_4$ decarboxylating enzymes, PEP carboxykinase and malic enzyme, which catalyze the gluconeogenic conversion of oxaloacetate to PEP and the conversion of malate to pyruvate, respectively (Fig. 1). To achieve a full understanding of these enzymatic reactions and their functions, it is important to gain insight into their activities in vivo. However, the presence of cyclic and parallel reactions prevents reliable estimation of the in vivo fluxes if we use the approach of

GLUCOSE

Pentose Phosphate Pathway

Glycolysis

TCA Cycle
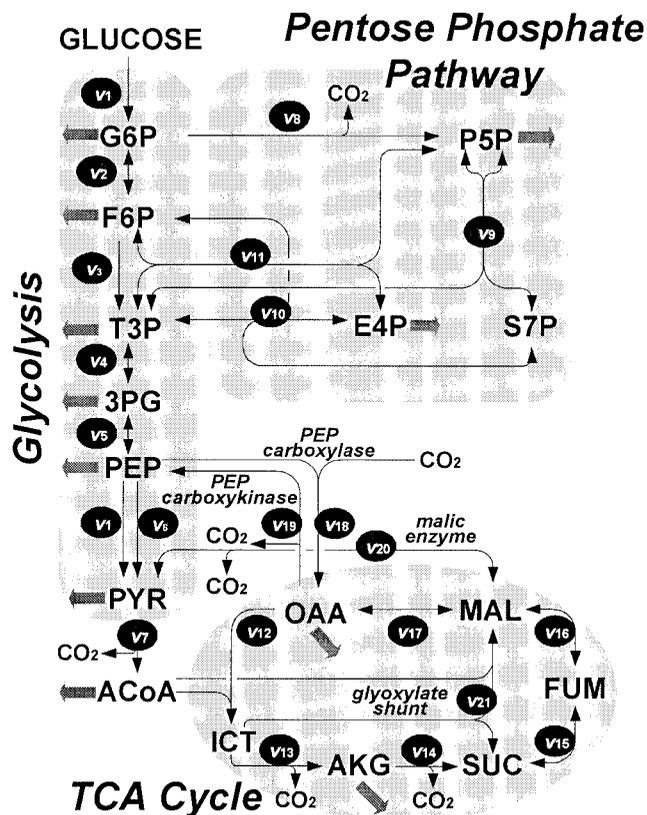
Figure 1. Bioreaction network of *E. coli* central carbon metabolism. Arrows indicate the physiological direction of reactions. Fluxes to biomass building blocks are indicated by dark gray arrows. Abbreviations: G6P, glucose-6-phosphate; F6P, fructose-6-phosphate; T3P, triose-3-phosphate; 3PG, 3-phosphoglycerate; PEP, phosphoenolpyruvate; PYR, pyruvate; ACoA, acetyl-coenzyme A; P5P, pentose phosphates; S7P, seduheptulose-7-phosphate; E4P, erythrose-4-phosphate; OAA, oxaloacetate; ICT, isocitrate; AKG, α-ketoglutarate; SUC, succinate; FUM, fumarate; MAL, malate.

metabolite balancing within a stoichiometric model of cellular metabolism (Hua et al., 2001; Vallino and Stephanopoulos, 1993). Moreover, the intracellular reaction rates cannot be usually inferred from in vitro enzyme assays directly due to effectors that may modify the activity of enzymes. It is also questionable to estimate the in vivo metabolic fluxes based on the comparison of the overexpression or deletion mutants because the fluxes analyzed by this approach do not represent the natural situation and cells may react to the mutation by drastically changing the intracellular fluxes (Flores et al., 2002; Fraenkel, 1996).

A powerful approach for accurately quantifying the intracellular fluxes in a complex metabolic network is based on ^{13}C-labeling experiment followed by measurements of the isotopomers using either nuclear magnetic resonance (NMR) or mass spectrometry (Gombert et al., 2001; Marx et al., 1995; Szyperski, 1998). These data are then used to distinguish the metabolic fluxes between alternative pathways. One particular type of labeling experiment is based on growing cells on the mixture of uniformly ^{13}C-labeled [U-$^{13}C_6$] and unlabeled glucose (Canonaco et al., 2001;

Maaheimo et al., 2001; Sauer et al., 1999). The resulting ^{13}C-labeling patterns of intracellular metabolites are analyzed by 2D NMR spectroscopy. Using flux ratio analysis, the observed multiplet intensities are transformed into the relative abundance of intact carbon fragments that originated from a single source of glucose source molecule. Since alternative pathways leading to the same metabolites yield different intact fragments, this method enables the identification of active pathways in a bioreaction network and the analysis of the ratios of intracellular fluxes.

In addition to direct interpretation of the 2D NMR data by flux ratio analysis, the isotopomer measurement data in combination with biomass composition and all extracellular flux data, can also be used for quantification of the intracellular fluxes in a metabolic network (Dauner et al., 2001a; Schmidt et al., 1997; Wiechert, 2001). Based on the balances of metabolites and isotopomers, a mathematical framework relating the metabolic fluxes with the isotopomer measurement data is constructed. The intracellular flux distribution is then estimated by finding a best fit to all the available data in an iterative fitting procedure. This method has been used successfully to estimate intracellular fluxes in complex reaction networks (Dauner et al., 2001b; Sauer et al, 1997; Wendisch et al., 2000).

In this study, we used the method of combining flux ratio analysis with metabolic flux analysis to quantitatively investigate the anaplerotic metabolism in *E.coli*. The influence of growth rates and PEP carboxykinase knockout on the anaplerotic fluxes was reported. Flux ratio analysis was used to identify the metabolic network structure of *E. coli* grown under different conditions, and the flux distribution in the identified bioreaction network was quantified by metabolic flux analysis. Integration of in vivo fluxes with measurements of intracellular metabolite concentrations and specific enzyme activities allowed insights into the regulatory mechanisms of anaplerotic metabolism. The in vivo regulations of PEP carboxykinase flux, PEP carboxylation, and glyoxylate shunt in *E.coli* are also discussed in the present study.

MATERIALS AND METHODS

Strains and Cultivation Conditions

In the present study, we used two *E. coli* strains: wild-type W3110 (F-λ- IN(*rrnD-rrnE*)1 *rph-1*) and a PEP carboxykinase knockout mutant JWK3366. The mutant strain was constructed by deleting *pck* gene from an *E. coli* K-12 derivative BW25113 (F-λ-*rph-1* Δ*araBAD*$_{AH33}$ *lacI*^{q} Δ*lacZ*$_{WJ16}$ *rrnB*$_{T14}$ Δ*rhaBAD*$_{LD78}$ *hsdR514*) using an established protocol (Datsenko and Wanner, 2000).

The organisms were grown on the glucose-limited chemostat culture medium containing (per liter): 5.0 g of glucose, 1.0 g of NH$_4$Cl, 2.7 g of (NH$_4$)$_2$SO$_4$, 6.8 g of Na$_2$HPO$_4$, 3.0 g of KH$_2$PO$_4$, 0.6 g of NaCl, 0.2 g of MgSO$_4$ · 7H$_2$O, 1.0 μg of thiamine HCl, 2.0 μL of poly-

propylene glycol 2000 as an antiform agent, and 10 mL of trace element solution (Sauer et al., 1999).

Chemostat cultivations were operated at 37°C in a 2-L bioreactor (BMJ-02PI, ABLE Co., Tokyo, Japan) with a working volume of 1 liter. The culture medium was continuously fed to the bioreactor at a dilution rate of 0.10, 0.32, or 0.55 h^{-1}, and the working volume was kept constant by withdrawing culture broth through a continuously operating pump. The pH of the culture was maintained at 7.0 by adding 2.0M NaOH. Agitation speed at 450 rpm and constant airflow of 1.0 L/min^{-1}ensured dissolved oxygen concentrations above 60% saturation. The oxygen and carbon dioxide concentrations in the bioreactor effluent gas were monitored by an exhaust gas analyzer (Off-Gas Jr. DEX-2562, ABLE Co., Tokyo, Japan).

Labeling experiments were started after the cultures reached steady state. The steady-state condition was ascertained when optical density at 600 nm (OD$_{600}$) and exhaust gas analysis remained constant for at least three volume changes. The unlabeled feed was replaced by an identical medium containing 4.5 g of unlabeled glucose and 0.5 g of [U-^{13}C$_6$]glucose (^{13}C, > 98%; Isotec, Miamisburg, OH) per liter. Biomass samples for NMR analysis were taken after two volume changes, so that 86% of the biomass was ^{13}C labeled, which was calculated based on the first-order washout kinetics.

Analytical Methods

Cell growth was monitored by measuring the optical density (OD$_{600}$). Cell dry weight was determined by collecting cell pellets from 100 mL of culture aliquots, washing once with distilled water, and drying at 85°C until constant weight.

Glucose in culture supernatants was determined using an enzymatic test kit (Roche Molecular Biochemicals, Mannheim, Germany). Organic acids in culture supernatants were detected by high-pressure liquid chromatography described previously (Hua et al., 2001). Acetate was also determined enzymatically using Roche test kit.

The macromolecular composition of cellular biomass was determined from dried cell pellets that were prepared in the same way as the dry cells for weight measurement. The contents of protein and glycogen were determined as described previously (Yang et al., 2000). Total RNA was quantified by measuring the absorbance at 260 nm with yeast tRNA as standard.

Enzyme Assays

Cells were harvested from chemostats by centrifugation, washed and resuspended in disruption buffer, which contained 200 mM Tris-HCl (pH7.6), 4 mM MgCl$_2$, and 2 mM dithiothreitol. Cell disruption was achieved by sonication using an ultrasonic disruptor (Tomy UD-201, Tokyo, Japan). After removing the cell debris by centrifugation, the supernatant was used for enzyme assays. The protein concentration of the extract was determined by the Lowry method with bovine serum albumin as a standard (Lowry et al., 1951).

The activity of PEP carboxylase was measured by monitoring the decrease in NADH concentration using malate dehydrogenase as a coupling enzyme (Petersen et al., 2001). PEP carboxykinase activity was assayed in the carboxylation direction (Petersen et al., 2001). NADP-dependent isocitrate dehydrogenase activity was determined by monitoring the increase in NADPH (Goldberg and Ellis, 1983). The change in NAD(P)H was monitored fluorimetrically at a 355 nm excitation, 460 nm emission wavelength pair by using a dual-scanning microplate spectrofluorometer (SPECTRAmax GEMINI XS, Molecular Devices Co., Sunnyvale, CA). Isocitrate lyase activity was assayed by the phenylhydrazine method (McFadden, 1969). Enzyme activities were determined in duplicate at two different concentrations of crude extract in the same assay. All results of enzyme activities presented here were averaged over at least four determinations, considering the corresponding standard deviation in each.

Determination of Intracellular Metabolite Concentrations

To rapidly quench the cell metabolism, 5 mL of culture suspension was cooled to 0°C in a −50°C methanol bath within 15–20 s. Cells were separated from the culture medium by centrifugation, and resuspended in cold 100% methanol immediately. Intracellular metabolites were extracted by addition of cold chloroform at neutral pH based on the method of de Koning and van Dam (1992). This extraction method ensured minimal degradation of labile metabolites. After extraction, the aqueous phase was carefully collected, dried, and resuspended in MiliQ water. Shortly before the determination of metabolite concentrations, the cell extracts were filtered through a 0.2 μm-pore-size filter to remove possible small precipitates. The samples were stored for up to 5 days at −20°C for further analysis. The unstable metabolites (e.g., acetyl-CoA and oxaloacetate) were determined within 6 h after the extracts were obtained.

Enzymatic determinations of the intracellular metabolites were performed on a microplate spectrofluorometer (SPECTRAmax GEMINI XS), following the changes in NAD(P)H fluorescence at the 355, 460-nm wavelength pair. The volume of the assay mixture was 200 μL. The concentrations of fructose 1,6-bisphosphate, 3-phosphoglycerate, PEP, pyruvate, acetyl-CoA, isocitrate, L-malate, α-ketoglutarate, oxaloacetate, L-aspartate, and adenine nucleotide (ATP and ADP) in the extracts were measured according to published protocols (Bergmeyer, 1984, 1985; Williamson and Corkey, 1969) with some modifications (such as the reduction of analytical volume). The value of the specific cell volume used for calculation of the intracellular concentrations was 1.77 μL mg$_{DW}$$^{-1}$ (Chassagnole et al., 2002). All the intracellular concentrations were presented as the average of at least three measurements, with the corresponding standard deviation.

NMR Spectroscopy

At the end of the labeling experiment, cells in 100 mL of culture were harvested by centrifugation. The cell pellets were washed once with 20 mM Tris-HCl (pH7.6), and hydrolyzed in 6 mL of 6M HCl for 12 h at 105°C. In the resulting hydrolysate were sixteen proteinogenic amino acids, since cysteine and tryptophan were oxidized and asparagines and glutamine were deaminated during the acid hydrolysis. The hydrolysate was filtered and evaporated to dryness. The dried material was then dissolved in 650 μL of 20 mM ^{2}HCl in ^{2}H$_2$O, filtered, and used for the NMR measurements.

The labeling patterns of amino acids and glycerol in the hydrolysates were determined by NMR spectroscopy. All the measurements were performed at 30°C and 400 MHz on a Bruker Avance 400 spectrometer (Bruker, Karlsruhe, Germany), and 2D proton-detected heteronuclear ^{13}C-^{1}H correlation ([^{13}C, ^{1}H]-COSY) spectra were recorded (Szyperski, 1995). For each labeling experiment, two spectra were measured: one focused on aliphatic carbons and the other for the aromatic rings. The measurement time of the aliphatic spectra was 15.5 h (data size 3072 × 1024 complex points; t_{1max} = 249 ms; t_{2max} = 128 ms), and the spectra of the aromatic resonance were recorded at 10.5 h (data size 2048 × 1024 complex points; t_{1max} = 360 ms; t_{2max} = 128 ms). The digital resolutions along ω_1 after linear prediction and zero-filling were 0.86 Hz/point for aliphatic spectra and 1.47 Hz/point for aromatic spectra. All NMR data processing was performed using the Bruker XWINNMR software. The relative abundances of singlet, doublet, and doublet of doublets signals were evaluated from the cross-section taken along the ^{13}C axis in a 2D spectrum (Yang et al., 2002).

The overall degree of ^{13}C labeling in the sample, P_1, was determined from the satellites of well-separated peaks in one-dimensional ^{1}H-NMR spectra (1.024-s acquisition time; 8-s interscan delay), and confirmed by analysis of the ^{13}C scalar coupling fine structure of leucine C$^\beta$. P_1 was 0.096 for all cases in this study.
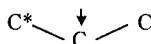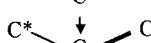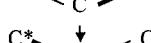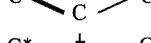
Flux Ratio Analysis

Forty-seven of ^{13}C scalar coupling fine structures for the 16 different amino acids and glycerol present in the hydrolysates were determined from a 2D NMR spectrum. The observed relative multiplet intensities (I values) were used to calculate the relative abundances of intact carbon fragments (f values) with the method of Szyperski (1995). The denotations of f are briefly given in Table I. These f values were calculated from the observed relative multiplet intensities, I, by Eq. (1).

$$\mathbf{f} = \mathbf{K}^{-1} \cdot \mathbf{I} \qquad (1)$$

The transformation matrix, $\mathbf{K}$, are composed of the probabilistic expressions that are functions of the degree of ^{13}C labeling at natural abundance, P_n = 0.01107, the over-

Table I. Denotation of f in flux ratio analysis.[a]

Carbon position	f	The fractions of molecules represented by f
Terminal		
	$f^{(1)}$	
	$f^{(2)}$	
Central in C$_3$ fragment[b]		
	$f^{(1)}$	
	$f^{(2a)}$	
	$f^{(2b)}$	
	$f^{(3)}$	

[a]According to the description in Szyperski (1995). Arrows indicate the observed carbon position. The carbon–carbon bonds that remain intact from a single glucose source molecule are shown in bold.
[b]The carbon with the asterisk exhibits the larger coupling with the observed carbon. In the case where the observed carbon has identical scalar coupling constants to the adjacent carbons, $f^{(2)}$ is the sum of $f^{(2a)}$ and $f^{(2b)}$.

all degree of ^{13}C labeling, P_1, and the fraction of [U-^{13}C$_6$]glucose to the total amount of glucose, P_f. Considering that the unlabeled biomass in bioreactor follows the first-order washout kinetics during the labeling experiment, P_1 can be calculated using Eq. (2).

$$P_1 = (1 - e^{-\mu \cdot t}) \cdot [P_s + (1 - P_s) \cdot P_n] + e^{-\mu \cdot t} \cdot P_n \qquad (2)$$

where t is the time elapsed between the initiation of labeling experiments and biomass harvesting for NMR measurements, and P_s the fraction of [U-^{13}C$_6$]glucose in the feed. Here we have $\mu \cdot t$ = 2 and P_s = 0.1. The P_1 value calculated from Eq. (2) was in good agreement with the value determined from 1D ^{1}H-NMR spectra. The fraction of labeled glucose to the total glucose, P_f, can be calculated from Eq. (3) considering the presence of unlabeled biomass in bioreactor.

$$P_f = (1 - e^{-\mu \cdot t}) \cdot P_s \qquad (3)$$

The probabilistic expressions, as described by Szyperski (1995), were used to calculate the components in the matrix $\mathbf{K}$, which denote the relative multiplet intensities arising from different intact carbon fragments. The matrices $\mathbf{K}$ used in this study are given by Eqs. (4) and (5) in Table II.

The relative abundances of intact carbon fragments in the amino acids and glycerol calculated from Eqs. (1), (4), and (5) were used to derive information on the origin of the precursor intermediates: pentose phosphates, erythrose 4-phosphate, triose phosphates, 3-phosphoglycerate, PEP, pyruvate, acetyl-CoA, α-ketoglutarate, oxaloacetate. Flux ratios through several key pathways in central metabolism of wild-type *E. coli* strains have been derived by Szyperski

Table II. The transformation matrix **K** for calculating f values by Eq. (1).[a]

Carbon position	**K**	
Terminal	$\mathbf{K}_{\text{term}} = \begin{bmatrix} K_s^{(1)} & K_s^{(2)} \\ K_d^{(1)} & K_d^{(2)} \end{bmatrix} = \begin{bmatrix} 0.904 & 0.104 \\ 0.096 & 0.896 \end{bmatrix}$	(4)
Central in C$_3$ fragment	$\mathbf{K}_{\text{central}} = \begin{bmatrix} K_s^{(1)} & K_s^{(2a)} & K_s^{(2b)} & K_s^{(3)} \\ K_{da}^{(1)} & K_{da}^{(2a)} & K_{da}^{(2b)} & K_{da}^{(3)} \\ K_{db}^{(1)} & K_{db}^{(2a)} & K_{db}^{(2b)} & K_{db}^{(3)} \\ K_{dd}^{(1)} & K_{dd}^{(2a)} & K_{dd}^{(2b)} & K_{dd}^{(3)} \end{bmatrix} = \begin{bmatrix} 0.819 & 0.094 & 0.094 & 0.102 \\ 0.086 & 0.811 & 0.010 & 0.001 \\ 0.086 & 0.010 & 0.811 & 0.001 \\ 0.009 & 0.085 & 0.085 & 0.896 \end{bmatrix}$	(5)

[a]The components in the matrix **K** were calculated with the probabilistic expressions described by Szyperski (1995). $K_s^{(1)}$ represents the relative intensity of the singlet signal arising from $f^{(1)}$, the fraction of molecules with neighboring carbons coming from different source molecules, and other components in matrix **K** are defined in analog ot $K_s^{(1)}$.

(1995) and Szyperski et al. (1996). To cope with the unpredictable changes in metabolic network structure due to genetic manipulations, the formalism derived to analyze wild-type metabolism needs to be extended. Here we present the equations that are required to investigate the anaplerotic metabolism [Eqs. (6)–(10) in Table III]. The derivation for the fraction of oxaloacetate synthesized via the glyoxylate shunt is given as follows.

Table III. The equations for calculation of the flux ratios involved in anaplerotic metabolism.[a]

Oxaloacetate from PEP[b]

$$X^{ppc} = X(\text{OAA} \leftarrow \text{PEP}) = \frac{f^{(2a)}\{\text{Asp} - \alpha\} + f^{(3)}\{\text{Asp} - \alpha\}}{f^{(2a)}\{\text{Phe} - \alpha, \text{Tyr} - \alpha\} + f^{(3)}\{\text{Phe} - \alpha, \text{Tyr} - \alpha\}}$$

$$= \frac{f^{(2a)}\{\text{Asp} - \beta\} + f^{(3)}\{\text{Asp} - \beta\}}{f^{2a}\{\text{Phe} - \alpha, \text{Tyr} - \alpha\} + f^{(3)}\{\text{Phe} - \alpha, \text{Tyr} - \alpha\}} \quad (6)$$

PEP from oxaloacetate[c]

$$X(\text{PEP} \leftarrow \text{OAA}) = \frac{f^{(2b)}\{\text{Phe} - \alpha, \text{Tyr} - \alpha\}}{f^{(2b)}\{\text{Asp} - \alpha\}} \quad (7)$$

Pyruvate from malate[d]

$$X^{lb}(\text{PYR} \leftarrow \text{MAL}) = \frac{f^{(2b)}\{\text{Ala} - \alpha\} - f^{(2b)}\{\text{Phe} - \alpha\}}{1 - f^{(2b)}\{\text{Phe} - \alpha\}} \quad (8)$$

$$X^{ub}(\text{PYR} \leftarrow \text{MAL}) = \frac{f^{(2b)}\{\text{Ala} - \alpha\} - f^{(2b)}\{\text{Phe} - \alpha\}}{f^{(2b)}\{\text{Asp} - \alpha\} - f^{(2b)}\{\text{Phe} - \alpha\}} \quad (9)$$

Oxaloacetate via glyoxylate shunt[e]

$$X^{glo} = \frac{f^{(2b)}\{\text{Asp} - \alpha\} - X^{ppc} \cdot (1 - 0.5 \cdot X^{exch}) \cdot f^{(2b)}\{\text{Phe} - \alpha\} - (1 - X^{ppc}) \cdot D}{0.5 \cdot (A + B) - D} \quad \text{or}$$

$$X^{glo} = \frac{f^{(2b)}\{\text{Asp} - \beta\} - X^{ppc} \cdot 0.5 \cdot X^{exch} \cdot f^{(2b)}\{\text{Phe} - \alpha\} - (1 - X^{ppc}) \cdot D}{0.5 \cdot (A + C) - D}$$

$A = 0.5 \cdot (f^{(2b)}\{\text{Leu} - \alpha\} + f^{(2b)}\{\text{Asp} - \alpha\} + f^{(3)}\{\text{Asp} - \alpha\})$

$B = (1 - 0.5 \cdot X^{exch}) \cdot (f^{(2b)}\{\text{Asp} - \beta\} + f^{(3)}\{\text{Asp} - \beta\}) + 0.5 \cdot X^{exch} \cdot f^{(2b)}\{\text{Leu} - \alpha\}$

$C = 0.5 \cdot X^{exch} \cdot (f^{(2b)}\{\text{Asp} - \beta\} + f^{(3)}\{\text{Asp} - \beta\}) + (1 - 0.5 \cdot X^{exch}) \cdot f^{(2b)}\{\text{Leu} - \alpha\}$

$D = 0.5 \cdot (f^{(2)}\{\text{Glu} - \beta\} + f^{(2b)}\{\text{Glu} - \gamma\})$

(10)

[a]See the denotation of f in Table 1 and abbreviations in Figure 1 legend.

[b]Equation (6) is derived based on the fact that only the reaction catalyzed by PEP carboxylase leads to the introduction of intact C2–C3 connectivities in oxaloacetate.

[c]Equation (7) is derived based on the fact that the intact C1–C2 fragments in the PEP pool originate from oxaloacetate via the PEP carboxykinase. Here PEP synthase is assumed to be inactive.

[d]lb = lower bound; ub = upper bound. The conversion of malate to pyruvate via the malic enzyme leads to excess intact C1–C2 fragment into the pyruvate pool when compared with the PEP pool, and upper bound is derived under the assumption that malate is entirely synthesized from oxaloacetate.

[e]See the derivation in the text.

If the glyoxylate shunt is inactive, the intact C1-C2 and C3-C4 fragments in oxaloacetate pool originate from α-ketoglutarate and PEP, yielding Eq. (11).

$$
\begin{aligned}
f^{(2b)}\{Asp - \alpha\} &= X^{ppc} \cdot f^{(2b)}\{Phe - \alpha\} \\
&\quad + (1 - X^{ppc}) \cdot 0.5 \cdot (f^{(2)}\{Glu - \beta\} \\
&\quad + f^{(2b)}\{Glu - \gamma\}) \\
f^{(2b)}\{Asp - \beta\} &= (1 - X^{ppc}) \cdot 0.5 \cdot (f^{(2)}\{Glu - \beta\} \\
&\quad + f^{(2b)}\{Glu - \gamma\}) \quad\quad (11)
\end{aligned}
$$

In the above equation, X^{ppc}, the fraction of oxaloacetate from PEP can be calculated using Eq. (6) in Table III, and the $(1 - X^{ppc})$ term is obtained by assuming full symmetrization of ^{13}C labeling patterns due to the symmetry of succinate or fumarate. However, the symmetrization of ^{13}C labeling patterns arising from reversible interconversion from oxaloacetate to fumarate is not considered. The fraction of oxaloacetate molecules that were at least once reversibly interconverted to fumarate, denoted by $X^{exch} = X(OAA \leftrightarrow FUM)$, is given by Eq. (12), which is derived based on the considerations that this reaction leads to the introduction of intact C4-C3-C2 fragments into oxaloacetate molecules due to the symmetry of fumarate.

$$
X^{exch} = X(OAA \leftrightarrow FUM) = \frac{2 \cdot f^{(3)}\{Asp - \beta\}}{f^{(3)}\{Asp - \alpha\} + f^{(3)}\{Asp - \beta\}}
$$
(12)

Thus, the symmetrization of ^{13}C labeling patterns arising from reversible interconversion from oxaloacetate to fumarate is considered, yielding Eq. (13).

$$
\begin{aligned}
f^{(2b)}\{Asp - \alpha\} &= X^{ppc} \cdot (1 - 0.5 \cdot X^{exch}) \cdot f^{(2b)}\{Phe - \alpha\} \\
&\quad + (1 - X^{ppc}) \cdot 0.5 \cdot (f^{(2)}\{Glu - \beta\} \\
&\quad + f^{(2b)}\{Glu - \gamma\}) \\
f^{(2b)}\{Asp - \beta\} &= X^{ppc} \cdot 0.5 \cdot X^{exch} \cdot f^{(2b)}\{Phe - \alpha\} \\
&\quad + (1 - X^{ppc}) \cdot 0.5 \cdot (f^{(2)}\{Glu - \beta\} \\
&\quad + f^{(2b)}\{Glu - \gamma\})
\end{aligned}
$$
(13)

Equation (13) is used to identify the activity of the glyoxylate shunt. If the glyoxylate shunt is inactive, Eq. (13) will be satisfied within experiment error, while the active glyoxylate shunt will result in obviously higher values of $f^{(2b)}\{Asp-\alpha\}$ and $f^{(2b)}\{Asp-\beta\}$ than the values calculated from Eq. (13).

If the glyoxylate shunt is active under the investigated conditions, excess intact C1-C2 and C3-C4 connectivities in oxaloacetate are introduced via the glyoxylate shunt, yielding Eq. (14).

$$
\begin{aligned}
f^{(2b)}\{Asp - \alpha\} &= X^{ppc} \cdot (1 - 0.5 \cdot X^{exch}) \cdot f^{(2b)}\{Phe - \alpha\} \\
&\quad + X^{glo} \cdot 0.5 \cdot (A + B) + (1 - X^{ppc} - X^{glo}) \cdot D \\
f^{(2b)}\{Asp - B\} &= X^{ppc} \cdot (1 - 0.5 \cdot X^{exch}) \cdot f^{(2b)}\{Phe - \alpha\} \\
&\quad + X^{glo} \cdot 0.5 \cdot (A + C) + (1 - X^{ppc} - X^{glo}) \cdot D \\
A &= 0.5 \cdot (f^{(2b)}\{Leu - \alpha\} + f^{(2b)}\{Asp - \alpha\} + f^{(3)}\{Asp - \alpha\})
\end{aligned}
$$
(14)

$$
\begin{aligned}
B &= (1 - 0.5 \cdot X^{exch}) \cdot (f^{(2b)}\{Asp - \beta\} + f^{(3)}\{Asp - \beta\}) \\
&\quad + 0.5 \cdot X^{exch} \cdot f^{(2b)}\{Leu - \alpha\}
\end{aligned}
$$

$$
\begin{aligned}
C &= 0.5 \cdot X^{exch} \cdot (f^{(2)}\{Asp - \beta\} + f^{(3)}\{Asp - \beta\}) \\
&\quad + (1 - 0.5 \cdot X^{exch}) \cdot f^{(2b)}\{Leu - \alpha\} \\
D &= 0.5 \cdot (f^{(2)}\{Glu - \beta\} + f^{(2b)}\{Glu - \gamma\})
\end{aligned}
$$

In Eqs. (10) and (14), A, B, and C represent the intact C1-C2 or C3-C4 fragments introduced via the glyoxylate shunt into oxaloacetate, and the symmetrization of ^{13}C labeling patterns due to reversible interconversion from malate to fumarate is also considered. Thus, the fraction of oxaloacetate synthesized via the glyoxylate shunt, X^{glo}, can be obtained using Eq. (10) in Table III.

The ratios of other metabolic fluxes can be assessed in a similar way, or found in Szyperski (1995). All results of flux ratios described in this article contained the standard error introduced by the experiment error, which was estimated from the analysis of redundant ^{13}C scalar coupling fine structures and the signal-to-noise ratio of the 2D NMR spectra.

Metabolic Flux Analysis

For the quantification of carbon fluxes in the central metabolism of *E. coli*, a bioreaction network was constructed as shown in Figure 1. It includes the reactions of glycolysis, pentose phosphate pathway, and the TCA cycle. Besides these pathways, other reactions have been included based on the results of flux ratio analysis (see the Results section for further details).

The carbon flux distribution in the bioreaction network was determined as a best fit to all extracellular flux measurements, the macromolecular biomass composition, and the relative intensities of the ^{13}C-^{13}C scalar coupling multiplets of the aforementioned 47 carbon positions of amino acids and glycerol determined by 2D [^{13}C, ^1H]-COSY. The flux quantification was performed by a least-squares parameter fitting approach in the mathematical framework described previously (Yang et al., 2002). Exchanges fluxes via reversible reactions were quantitatively considered in the flux calculations. Initially, the isotopomer balances of all metabolites in the bioreaction network are calculated from a random initial flux distribution. Relative ^{13}C multiplet intensities are then simulated from this isotopomer distribution and compared to the experimental values. The quality of the fit was judged by the χ^2 (error) value. Multiple calculations were performed from different random starting points, and the best solution that was reproducibly attained was presented as the estimated result of flux distribution. A statistical error analysis of the estimated fluxes was included in the calculations. Moreover, the flux estimates were compared with the results of flux ratio analysis, since both methods employed are very different and thus flux ratio analysis can serve as an independent verification of the flux estimates. In addition, the calculation of the flux distribution in the *pck* deletion mutant was performed without any constraint on the flux through PEP carboxykinase.

RESULTS

Growth Parameters

In this study, continuous cultivation in glucose-limited chemostats was used to determine the growth parameters of *E. coli* wild-type W3110 and the PEP carboxykinase knockout mutant JWK3366. The wild-type strain was also examined at different dilution rates to investigate the changes in carbon metabolism related to cell growth. The experimentally determined growth parameters are summarized in Table IV. Both strains converted glucose quantitatively to biomass and CO_2 without any significant byproduct formation. In accordance with this observation, the carbon balances were closed within experimental errors. Abolition of PEP carboxykinase activity by deletion of the corresponding gene *pck* resulted in a significantly increased biomass yield on glucose and a drastic reduction in CO_2 production rates.

The macromolecular composition of biomass is known to change with environmental conditions and growth rate. Hence, to obtain accurate information on the specific precursor requirements for subsequent flux analysis, we determined the relative fraction of the major biomass components of *E. coli:* protein, RNA, and glycogen. While glycogen was negligible (about 1.4%) under all conditions, the protein content was 70% ± 7%, 68% ± 8%, 65% ± 5%, and the RNA content was 7% ± 1%, 8% ± 1%, 12% ± 1% in the wild-type chemostat cultures at dilution rates of 0.10, 0.32, and 0.55 h^{-1}, respectively. As expected, the RNA content increased with the growth rate. The contents of protein and RNA in the *pck* deletion mutant were 68% ± 8% and 7% ± 1%, respectively. Hence, deletion of *pck* was found to have no significant impact on the macromolecular biomass composition. The remaining fraction of biomass was assigned according to Dauner and Sauer (2001).

Network Identification by Flux Ratio Analysis

The cells from [U-$^{13}C_6$]glucose labeling experiments were harvested, subjected to hydrolysis, and the relative abundances of ^{13}C-^{13}C scalar coupling multiplets of amino acids and glycerol in the hydrolysates were analyzed by 2D [^{13}C, ^{1}H]-COSY (Fig. 2). NMR data were interpreted using flux ratio analysis, yielding information on the origin of key metabolites in the central metabolism (Table V). The results of flux ratio analysis allowed identification of the network of active reactions and conclusion on the ratios of some carbon fluxes.

The flux ratio analysis of wild-type W3110 showed the activity of PEP carboxykinase and malic enzyme that are generally considered to be inactive in *E. coli* grown on glucose (Table V). The gluconeogenic PEP carboxykinase was active even at a very high growth rate (0.55 h^{-1}). The glyoxylate shunt consisting of isocitrate lyase and malate synthase was found to be inactive in W3110, because Eq. (13) was satisfied within experiment error. The anaplerotic PEP carboxylase was responsible for about half of the oxaloacetate molecules synthesized in wild-type *E. coli* (Table V). Comparing the results of flux ratio analysis of wild-type *E. coli* at different growth rates, very similar flux ratio patterns were found. The only exception was the reduction in both the fraction of PEP molecules originating from oxaloacetate and the fraction of pyruvate arising from malate caused by an increase in growth rates (Table V). In addition, the flux ratios for W3110 obtained in this study were almost identical to those reported for *E. coli* MG1655 (Sauer et al., 1999) and those of the parent strain BW25113 used for PEP carboxykinase knockout (data not shown), suggesting negligible interstrain difference in central carbon metabolism.

The results in Table V showed the absence of PEP molecules originating from oxaloacetate in the *pck* deletion mutant. This information was obtained from the probabilistic interpretation of the ^{13}C-^{13}C scalar coupling fine structure of Phe-α in the [^{13}C, ^{1}H]-COSY spectra. As can be seen in Figure 2, the scalar coupling multiplets of Phe-α, which represent the labeling in PEP, showed absence of the db component for the *pck* deletion mutant, indicating the lack of intact C1-C2 fragments in PEP due to the abolishment of PEP carboxykinase activity. This result also excluded the possibility of an active PEP synthase in the *pck* deletion mutant and confirmed the activity of PEP carboxykinase in wild-type *E. coli* grown on glucose.

A decrease in the fraction of oxaloacetate molecules arising from PEP was observed for the *pck* deletion mutant

Table IV. Growth parameters of glucose-limited chemostat cultures of *E. coli* wild-type W3110 and PEP carboxykinase-deficient mutant JWK3366.[a]

	E. coli strain at growth rate			
Growth parameters	W3110 (0.10 h^{-1})	W3110 (0.32 h^{-1})	W3110 (0.55 h^{-1})	JWK3366 (0.10 h^{-1})
Biomass yield (g g^{-1})	0.40 ± 0.02	0.44 ± 0.02	0.48 ± 0.03	0.46 ± 0.02
Glucose uptake rate (mmol g^{-1} h^{-1})	1.4 ± 0.1	4.0 ± 0.2	6.4 ± 0.3	1.2 ± 0.1
O_2 uptake rate (mmol g^{-1} h^{-1})	4.0 ± 0.7	10.7 ± 1.6	16.3 ± 2.4	2.7 ± 0.5
CO_2 evolution rate (mmol g^{-1} h^{-1})	4.2 ± 0.4	11.1 ± 1.2	16.6 ± 1.8	2.9 ± 0.3
C balance (%)	99 ± 7	103 ± 8	104 ± 8	97 ± 7

[a]The parent strain used for PEP carboxykinase knockout, *E. coli* BW25113, exhibited almost the same growth parameters as W3110.
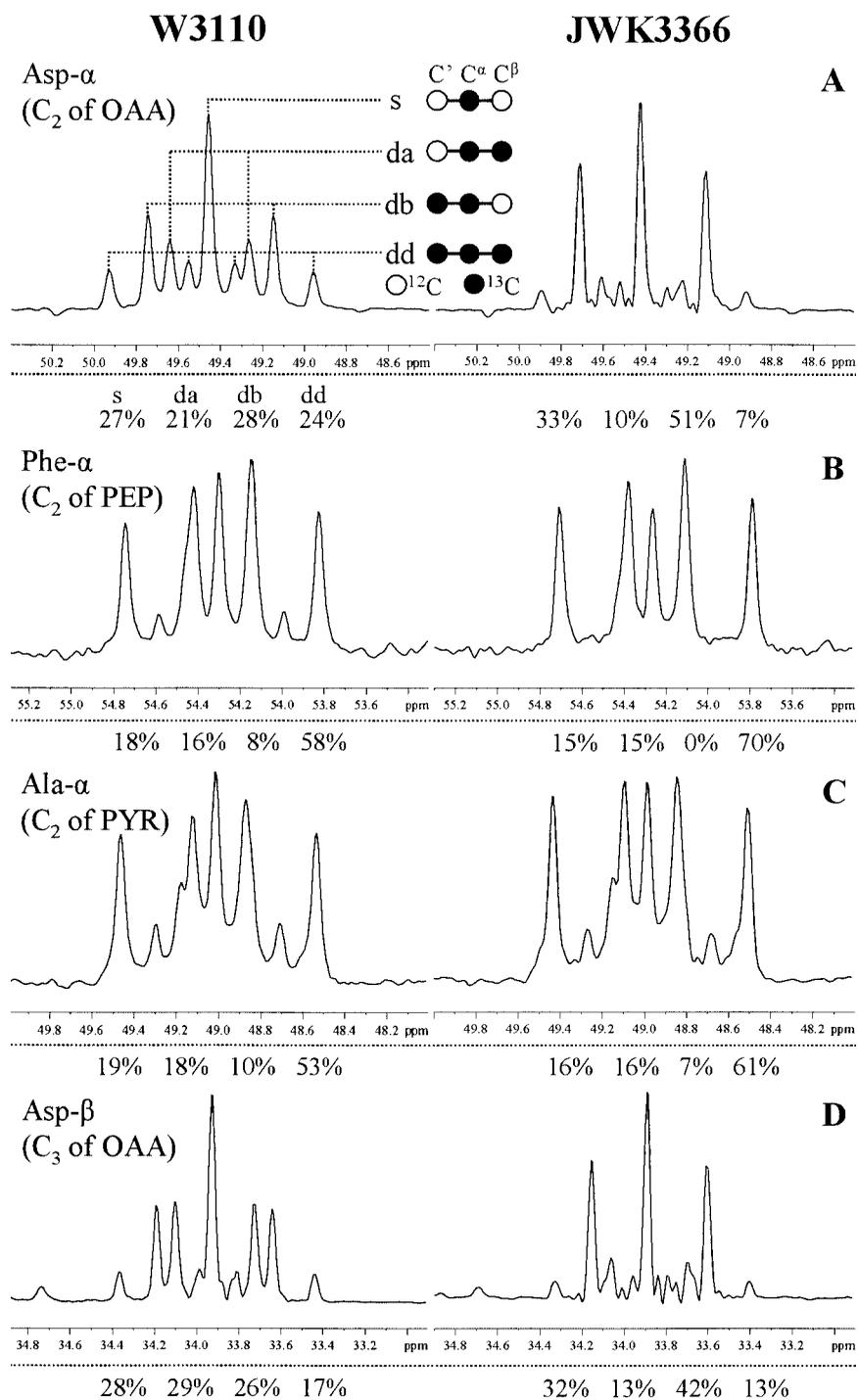
Figure 2. ^{13}C-^{13}C scalar coupling multiplets for the amino acids isolated from *E. coli* W3110 (left) and PEP carboxykinase-deficient mutant JWK3366 (right) cultivated at the growth rate of 0.10 h^{-1}. These signals were extracted from the $\omega_1(^{13}$C) cross-sections in 2D [^{13}C,^{1}H]-COSY spectra. A: aspartate C$^{\alpha}$; B: phenylalanine C$^{\alpha}$; C: alanine C$^{\alpha}$; D: aspartate C$^{\beta}$. In the panels are given the metabolic intermediates from which the carbon atoms are derived. As indicated in (A), the multiplets consist of a singlet (s), a doublet with a small coupling constant (da), a doublet split by a larger coupling constant (db), and a doublet of doublets (dd). The relative abundances of the multiplet components that reflect the metabolic state of the organism are given in each panel. For abbreviations, see the legend to Figure 1.

when compared to the wild-type strain (Table V). This can also be qualitatively assessed from direct inspection of the ^{13}C-^{13}C scalar coupling fine structure of Asp-α (Fig. 2). The abundances of the da and dd components in the multiplets of Asp-α relate to the oxaloacetate molecules (the direct pre-cursor of Asp) that possess intact C2-C3 connectivities. Since the intact C2-C3 fragments in oxaloacetate can be introduced only by the anaplerotic reaction of PEP carbox-ylation, the abundances of the da and dd components reflect the in vivo activity of the PEP carboxylase. The abundances

Table V. Origins of metabolic intermediates in chemostat cultures of *E. coli* W3110 and PEP carboxykinase-deficient mutant JWK3366 as determined by flux ratio analysis.

	% of Total pool in *E. coli* strain at growth rate			
Metabolite	W3110 (0.10 h⁻¹)	W3110 (0.32 h⁻¹)	W3110 (0.55 h⁻¹)	JWK3366 (0.10 h⁻¹)
P5P from G6P (lb)	17 ± 2	23 ± 2	21 ± 2	13 ± 2
P5P from T3P + S7P	82 ± 2	76 ± 2	78 ± 2	87 ± 2
P5P from E4P	35 ± 2	27 ± 2	19 ± 2	31 ± 2
OAA from PEP	56 ± 2	53 ± 3	48 ± 2	18 ± 3
PEP from OAA	28 ± 3	19 ± 3	11 ± 2	0 ± 2
PYR from MAL (lb)	2 ± 2	0 ± 2	0 ± 2	7 ± 3
PYR from MAL (ub)	8 ± 4	0 ± 2	0 ± 2	14 ± 3
ACoA from PYR	>98	>99	>98	>98
AKG from OAA + ACoA	>97	>98	>98	>97
OAA exchanged to FUM	76 ± 10	65 ± 10	72 ± 8	94 ± 14
OAA via glyoxylate shunt	_ᵇ	_ᵇ	_ᵇ	38 ± 12

ᵃFor abbreviations, see Figure 1 legend. lb = lower bound; ub = upper bound.

ᵇThe glyoxylate shunt was found to be inactive in W3110, because Eq. (13) was satisfied within experiment error. For these cases, the ratio values calculated from Eq. (10) have very large error values due to the division by a very small number.

of the da and dd components were significantly lower for the *pck* deletion mutant than those for the wild-type *E. coli* (Fig. 2), indicating a smaller fraction of oxaloacetate synthesized from the anaplerotic reaction of PEP carboxylation in the mutant.

Finally, the activity of the glyoxylate shunt in the *pck* deletion mutant was identified by flux ratio analysis (Table V). Visual inspection of the ¹³C multiplets of Asp-α and Asp-β revealed a surprisingly high abundance of the db component for the *pck* deletion mutant (Fig. 2). Using flux ratio analysis, it was found that the intact C1-C2 and C3-C4 fragments in oxaloacetate could not be derived entirely from the TCA cycle, and excess intact C1-C2 and C3-C4 connectivities were introduced via the glyoxylate shunt in the *pck* deletion mutant. That is, for this case, the value of the left side of Eq. (13) is significantly higher than the value of the right side. Hence, the flux ratio analysis showed evidence of the in vivo activity of the glyoxylate shunt, which is normally required for growth on carbon sources such as acetate or fatty acids and generally considered to be repressed in *E. coli* grown on glucose. Using Eq. (10), it was found that more than one third of oxaloacetate molecules were synthesized via the glyoxylate shunt in the PEP carboxykinase-deficient mutant (Table V). Consequently, the results of flux ratio analysis revealed that abolishment of PEP carboxykinase activity led to the reduced in vivo activity of anaplerotic PEP carboxylase and the activation of the glyoxylate shunt.

Intracellular Metabolic Fluxes

To obtain higher resolution on the intracellular fluxes, the relative abundances of ¹³C-¹³C scalar coupling multiplets

(data not shown), the determined biomass composition, and the extracellular flux data (Table IV) were combined for flux quantification. Based on the results of flux ratio analysis, the reactions catalyzed by PEP carboxylase, PEP carboxykinase, and malic enzyme were included in the bioreaction network for metabolic flux analysis. Moreover, since flux ratio analysis provided direct evidence for the activity of the glyoxylate shunt in the *pck* deletion mutant, this pathway was considered for quantification of the intracellular fluxes in the mutant cells. The intracellular flux distribution was then determined as the best fit to all the available measurement data using a parameter fitting approach.

Figure 3 shows the intracellular flux distributions in *E. coli* wild-type W3110 grown at different dilution rates. These carbon fluxes represent estimates for in vivo enzyme activities. It can be seen that in wild-type *E. coli*, there is a great interchange between PEP and oxaloacetate. The anaplerotic reaction catalyzed by PEP carboxylase replenished the TCA cycle with a carbon flux of 94%, while the backflow through the PEP carboxykinase was 67% at
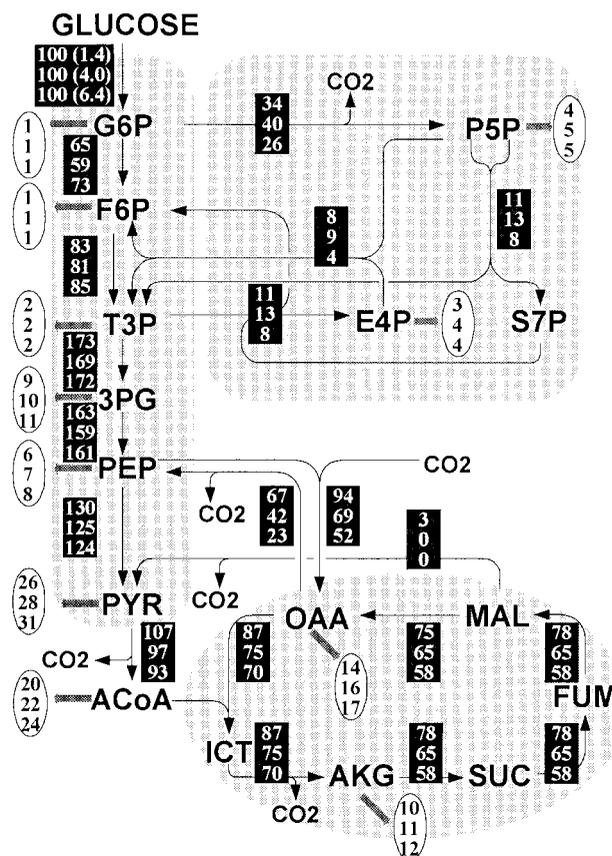
Figure 3. Metabolic flux distributions in chemostat cultures of *E. coli* W3110. Numbers in dark rectangles represent the determined net fluxes at dilution rates of 0.10 (top), 0.32 (middle) and 0.55 h⁻¹ (bottom). Flux values are relative to the specific glucose uptake rate that is given in parentheses in mmol g$_{DW}$⁻¹ h⁻¹. Arrows indicate the direction of the determined fluxes. Numbers in white ovals represent the fluxes of withdrawal of precursor metabolites for biomass production. For abbreviations, see Figure 1 legend.

the dilution rate of 0.10 h^{-1}. The in vivo activity of the gluconeogenic PEP carboxykinase was very high, and the backward flux from the TCA cycle to glycolysis carried by PEP carboxykinase was 23% of the total glucose consumed even at the dilution rate of 0.55 h^{-1}. As can be seen in Figure 3, different growth rates had little influence on the overall flux distribution. The only differences were the reduced fluxes through the TCA cycle (ν_{12-17}) and the simultaneous decrease in the fluxes through the PEP carboxylase and PEP carboxykinase at the higher growth rates. In addition, the malic enzyme flux was 3% at the low dilution rate (0.10 h^{-1}) and almost negligible at higher dilution rates.

The flux ratio analysis provided qualitative or semiquantitative evidence that knockout of PEP carboxykinase in *E. coli* results in a reduced activity of PEP carboxylase and the activation of the glyoxylate shunt. To quantitatively investigate the metabolic flux responses to the knockout, metabolic flux analysis was performed for quantifying the intracellular fluxes in the *pck* deletion mutant. The constraint on the flux through PEP carboxykinase was not included in the computation. As shown in Figure 4, the flux analysis confirmed that no decarboxylation of oxaloacetate to PEP was present in the *pck* deletion mutant. Consequently, the PEP carboxykinase knockout can be identified by the comprehensive flux analysis method.

As can be seen in Figure 4, the carbon flux through PEP carboxylase was decreased to 16% in the PEP carboxykinase-deficient *E. coli*. Furthermore, the glyoxylate shunt was activated due to *pck* deletion. Twenty-three percent of the isocitrate was funneled into the glyoxylate shunt, and 77% was converted further in the TCA cycle. The malate synthesized by the glyoxylate shunt (34% carbon flux) served to replenish the carbon skeletons withdrawn from the TCA cycle for biosynthesis. These results indicate that due to abolishment of PEP carboxykinase activity in the *pck* deletion mutant, the PEP carboxylase cannot solely fulfill the anaplerotic function, and both PEP carboxylase and glyoxylate shunt serve to replenish the TCA cycle.

The estimated flux distributions allow the calculation of the balance of NADPH, which is required for biomass formation and produced by the oxidative pentose-phosphate pathway (ν_8) and isocitrate dehydrogenase reaction (ν_{13}). According to our calculation, the NADPH imbalance is observed for all cultures. This is probably due to the interconversion between NADPH and NADH catalyzed by the transhydrogenase, which has been shown to be active in *E. coli* (Canonaco et al., 2001). The transhydrogenase flux converting NADPH to NADH is found to be 21%, 7%, −41% for wild-type *E. coli* at the dilution rates of 0.10, 0.32, 0.55 h^{-1}, and −39% for the *pck* deletion mutant, respectively.

The flux estimates in Figures 3 and 4 were obtained from at least 10 independent flux calculations, which were initiated from different random starting points. The independently calculated flux solutions turned out to be very similar, and the flux solutions with the lowest χ^2 values are shown in Figures 3 and 4. These χ^2 values were 69, 68, 49
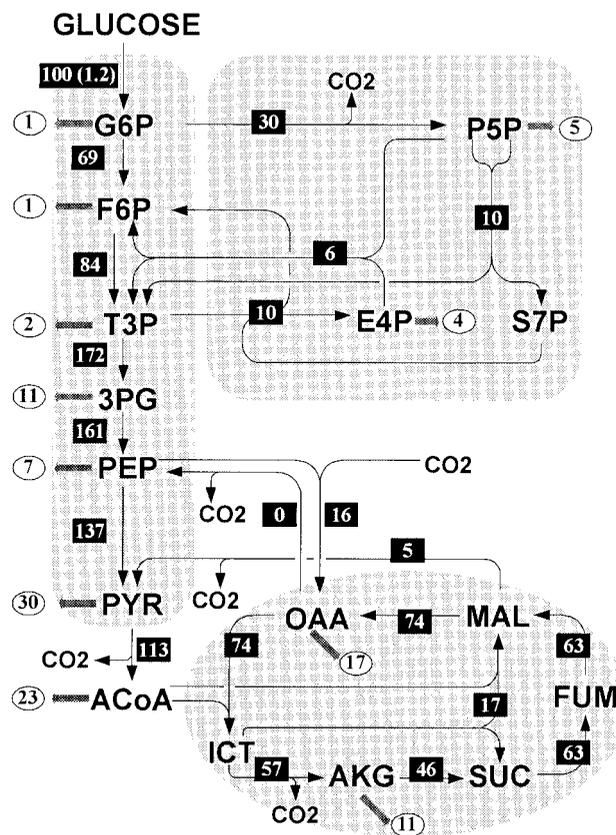
Figure 4. Metabolic flux distribution in PEP carboxykinase-deficient *E. coli* JWK3366 grown at the dilution rate of 0.10 h^{-1}. Numbers in dark rectangles represent the determined net fluxes. Flux values are relative to the specific glucose uptake rate that is given in parentheses in mmol gDW^{-1} h^{-1}. Arrows indicate the direction of the determined fluxes. Numbers in white ovals represent the fluxes of withdrawal of precursor metabolites for biomass production. For abbreviations, see the legend to Figure 1.

for wild-type *E. coli* at the dilution rates of 0.10, 0.32, 0.55 h^{-1}, and 92 for the *pck* deletion mutant, respectively. The low χ^2 values imply that the estimated fluxes fit well to the experimentally determined data and thus provide a reliable description of the metabolic processes in *E. coli.*

The flux solutions were also subjected to statistical error analysis based on Monte Carlo simulations (Schmidt et al., 1999; Yang et al., 2002). For most fluxes we obtained 90% confidence intervals that were less than 8% of the estimated flux. One exception was the oxidative pentose-phosphate pathway flux (ν_8), for which 90% confidence intervals were less than 25%. Finally, the flux estimates were compared with the flux ratios that were independently calculated from the flux ratio analysis. For example, from the estimated flux distribution in the *pck* deletion mutant (Fig. 4), the fraction of oxaloacetate arising from PEP and the fraction of oxaloacetate synthesized via the glyoxylate shunt were calculated to be 18% and 42%, respectively. The calculated values were in very good agreement with the results of flux ratios shown in Table V despite the differences in both methods employed, providing further evidence for the reliability of our flux estimates.

Enzyme Activities and Intracellular Metabolite Concentrations

The enzyme activities involved in the anaplerotic metabolism were determined for four chemostat cultivations. As shown in Table VI, the enzyme activity measurements confirmed that no PEP carboxykinase activity could be detected in the *pck* deletion mutant. Abolishment of PEP carboxykinase activity had no significant impact on the specific activity of PEP carboxylase (Table III), while the flux analysis revealed that the intracellular flux through PEP carboxylase was significantly reduced in the *pck* deletion mutant (Fig. 4). These observations indicate that the flux reduction of PEP carboxylase in the *pck* deletion mutant results from activity-level regulation, i.e., the flux is regulated by varying concentrations of substrates, activators, or inhibitors. The specific activity of isocitrate lyase cannot be detected in the wild-type *E. coli*, while the *pck* deletion mutant exhibited an isocitrate lyase activity of 167 nmol $mg_{protein}^{-1}$ min^{-1} and a more than sixfold decrease in the isocitrate dehydrogenase activity when compared to the wild-type strain (Table VI).

From Table VI, no significant changes in the specific activities of the investigated enzymes were found except the increased activity of anaplerotic PEP carboxylase at higher growth rates. In addition, it was found that the presence of acetyl-CoA in the assay mixture increased the PEP carboxylase activity by 10–20-fold. This is consistent with the findings of Izui et al. (1981) that the activity of *E. coli* PEP carboxylase is very low without any activator and acetyl-CoA is the most powerful activator.

To investigate the correlations of in vivo anaplerotic enzyme activities with the pool sizes of intracellular metabolites, we determined the intracellular concentrations of anaplerotically relevant metabolites (Table VII). Measured metabolites included fructose 1,6-bisphosphate, 3-phosphoglycerate, PEP, pyruvate, acetyl-CoA, isocitrate, L-malate, α-ketoglutarate, oxaloacetate, L-aspartate, ATP, and ADP. The results presented in Table VII show that knockout of PEP carboxykinase has no significant impact on the pool sizes of most intracellular metabolites. The only exceptions are a slight reduction in acetyl-CoA pool size, a lower oxaloacetate concentration and increased concentrations of iso-

Table VI. Specific enzymatic activities in chemostat cultures of *E. coli* W3110 and PEP carboxykinase-deficient mutant JWK3366.

Enzyme activity (nmol min^{-1} mg protein^{-1})	*E. coli* strain at growth rate			
	W3110 (0.10 h^{-1})	W3110 (0.32 h^{-1})	W3110 (0.55 h^{-1})	JWK3366 (0.10 h^{-1})
PEP carboxykinase	28 ± 5	36 ± 6	33 ± 6	<1.2
PEP carboxylase	3.5 ± 0.6	19 ± 3	23 ± 4	2.9 ± 0.6
PEP carboxylase (acetyl-CoA added)[a]	67 ± 12	270 ± 30	350 ± 40	56 ± 10
Isocitrate dehydrogenase	630 ± 90	760 ± 120	720 ± 110	98 ± 14
Isocitrate lyase	0	0	0	170 ± 12

[a]Acetyl-coenzyme A (1 m*M*) was added to the assay mixtures.

Table VII. Intracellular metabolite concentrations in chemostat cultures of *E. coli* W3110 and PEP carboxykinase-deficient mutant JWK3366.[a]

Metabolite concentrations (m*M*)	*E. coli* strain at growth rate			
	W3110 (0.10 h^{-1})	W3110 (0.32 h^{-1})	W3110 (0.55 h^{-1})	JWK3366 (0.10 h^{-1})
FBP	0.92 ± 0.11	0.78 ± 0.14	0.46 ± 0.04	1.41 ± 0.21
3PG	1.67 ± 0.21	0.68 ± 0.06	0.42 ± 0.04	1.79 ± 0.16
PEP	0.88 ± 0.14	0.17 ± 0.04	0.06 ± 0.01	1.28 ± 0.18
PYR	1.64 ± 0.32	0.48 ± 0.07	0.28 ± 0.04	1.42 ± 0.28
ACoA	1.42 ± 0.35	1.02 ± 0.21	0.68 ± 0.14	0.80 ± 0.12
ICT	<0.03	<0.03	<0.03	0.05 ± 0.01
AKG	2.54 ± 0.24	1.02 ± 0.09	0.30 ± 0.03	2.13 ± 0.27
MAL	0.07 ± 0.01	0.06 ± 0.01	0.07 ± 0.01	0.15 ± 0.02
OAA	1.07 ± 0.21	0.77 ± 0.14	0.49 ± 0.07	0.38 ± 0.06
Asp	3.95 ± 0.80	3.45 ± 0.67	2.28 ± 0.41	3.36 ± 0.65
ATP	0.94 ± 0.22	1.01 ± 0.21	1.20 ± 0.25	1.22 ± 0.31
ADP	0.32 ± 0.09	0.51 ± 0.14	0.63 ± 0.17	1.21 ± 0.35

[a]For abbreviations, see Figure 1 legend.

citrate, malate, and ADP in the *pck* deletion mutant when compared to wild-type *E. coli*. On the other hand, the increase in growth rates resulted in higher intracellular concentrations of ATP and ADP, almost unchanged malate pool size, and decreased concentrations of the other metabolites. From the data presented in Table VII the ATP/ADP concentration ratio can be calculated but should be treated with care, because the ADP concentrations have large measurement errors. Isocitrate concentrations are low in *E. coli* W3110 and only an upper bound of its pool size (0.03 m*M*) is given.

DISCUSSION

In vivo Regulation of Phosphoenolpyruvate Carboxykinase Flux

The primary objective of the present study is the quantitative elucidation of the responses of in vivo anaplerotic fluxes to the changes in growth rates and PEP carboxykinase knockout in *E. coli*. For this purpose, the complementary methods of flux ratio analysis and metabolic flux analysis were used for the quantitative inspection of metabolism. The results show a high in vivo activity of gluconeogenic PEP carboxykinase in wild-type *E. coli* grown on glucose (Table V and Fig. 3). This indicates the operation of an ATP-dissipating futile cycling via PEP carboxylase and ATP-consuming PEP carboxykinase. This futile cycle activity was reduced in faster growing *E. coli* cells. Assuming 1.3 ATP molecules formed per atom of oxygen, i.e., P/O ratio 1.3 (Varma and Palsson, 1995), it can be calculated from the carbon fluxes presented in Figure 3 that the ATP dissipation for the futile cycling via PEP carboxykinase is 8.2%, 5.7%, 3.5% of total ATP produced during the growth of wild-type *E. coli* at the dilution rates of 0.10, 0.32, 0.55 h^{-1}, respectively. Deletion of *pck* led to a significant decrease in carbon dioxide production and oxygen uptake

(Table IV), which is consistent with the reduced energy demands by abolishment of the futile cycling via PEP carboxykinase.

Since a remarkable fraction of the available ATP is consumed for the futile cycling via PEP carboxykinase, it is speculated that special biological functions are supported by this enzyme during the growth of *E. coli* on glucose. To understand the significance of PEP carboxykinase activity, we investigated the in vivo regulation of the flux through PEP carboxykinase by integrating the measured results of in vivo fluxes and intracellular metabolite concentrations.

The kinetics of the PEP carboxykinase in *E. coli* is assumed to follow the rapid equilibrium mechanism based on the study of Krebs and Bridger (1980). Thus, we can express the rate equation for this enzyme by Eq. (15) in Table VIII. Using Eq. (15), the maximal rate, v_{max}, of PEP carboxykinase was calculated from the measured metabolite concentrations (Table VII) and determined in vivo flux value. As shown in Figure 3, the carbon flux through PEP carboxykinase was 0.93, 1.70, 1.46 mmol g^{-1} h^{-1}during the growth of wild-type *E. coli* at the dilution rates of 0.10, 0.32, 0.55 h^{-1}, respectively. Thus, the v_{max} values calculated from Eq. (15) were 13.6, 11.6, 9.5 mmol g^{-1} h^{-1},

respectively. These v_{max} values show no significant changes between different dilution rates, which is in agreement with the measured data of specific enzyme activities (Table VI). Furthermore, it was found that the in vivo PEP carboxykinase fluxes relative to their maximal rate values (v/v_{max}) were less than 15%. These results indicate that the in vivo regulation of the flux through PEP carboxykinase according to growth requirements is exerted at the activity level via the changes in metabolite concentrations.

Since the intracellular ATP and ADP concentrations in *E. coli* are much higher than their respective K and K_i values (Table VII), Eq. (15) can be simplified as Eq. (16) in Table VIII. Equation (16) was used to assess the dependence of the PEP carboxykinase flux on the ATP/ADP concentration ratio and the sensitivities towards the PEP and oxaloacetate concentrations. It can be seen from Figure 5A that the flux is insensitive to alterations of the [ATP]/[ADP] ratio unless the latter falls below 1.0, while the measured [ATP]/[ADP] ratio is greater than 1.9 in wild-type *E. coli* (Table VII). On the other hand, Figure 5B shows that the flux sensitivities towards the PEP and oxaloacetate pool sizes are high when the concentrations of PEP and oxaloacetate are less than 1 m*M* and 2 m*M*, respectively. Interestingly, the measured

Table VIII. Kinetic rate equation of PEP carboxykinase.[a]

$$v_{pck} = \cfrac{v_{max}[OAA][ATP]}{\left(\begin{array}{l} K_{i,ATP}K_{OAA}[ATP] + K_{ATP}[OAA] + [OAA][ATP] \\[2mm] + \dfrac{K_{i,ATP}K_{OAA}[PEP]}{K_{i,PEP}} + \dfrac{K_{i,ATP}K_{OAA}[ADP]}{K_{i,ADP}} \\[2mm] + \dfrac{K_{i,ATP}K_{OAA}[PEP][ADP]}{K_{PEP}K_{i,ADP}} + \dfrac{K_{i,ATP}K_{OAA}[ATP][PEP]}{K_{i,PEP}K_{I,ATP}} \\[2mm] + \dfrac{K_{i,ATP}K_{OAA}[OAA][ADP]}{K_{i,ADP}K_{I,OAA}} \end{array}\right)} \qquad (15)$$

$K_{ATP} = 0.06$ m*M* $\qquad K_{OAA} = 0.67$ m*M* $\qquad K_{PEP} = 0.07$ m*M*

$K_{i,ATP} = 0.04$ m*M* $\qquad K_{i,PEP} = 0.06$ m*M* $\qquad K_{i,ADP} = 0.04$ m*M*

$K_{I,ATP} = 0.04$ m*M* $\qquad K_{I,OAA} = 0.45$ m*M*

$$v_{pck} = v_{max}\cfrac{[OAA]\cdot\dfrac{[ATP]}{[ADP]}}{\left(\begin{array}{l} K_{OAA}\cdot\dfrac{[ATP]}{[ADP]} + [OAA]\cdot\dfrac{[ATP]}{[ADP]} + \dfrac{K_{i,ATP}K_{OAA}}{K_{i,ADP}} \\[2mm] + \dfrac{K_{i,ATP}K_{OAA}}{K_{PEP}K_{i,ADP}}\cdot[PEP] + \dfrac{K_{i,ATP}K_{OAA}}{K_{i,PEP}K_{I,ATP}}\cdot\dfrac{[ATP]}{[ADP]}\cdot[PEP] \\[2mm] + \dfrac{K_{i,ATP}K_{OAA}}{K_{i,ADP}K_{I,OAA}}\cdot[OAA] \end{array}\right)} \qquad (16)$$

where [ATP] $\gg K_{ATP}$, [ATP] $\gg K_{i,ATP}$ and [ADP] $\gg K_{i,ADP}$

[a]The kinetics of this enzyme is assumed to follow the rapid equilibrium mechanism based on the study of Kerbs and Bridger (1980). For abbreviations, see Figure 1 legend.
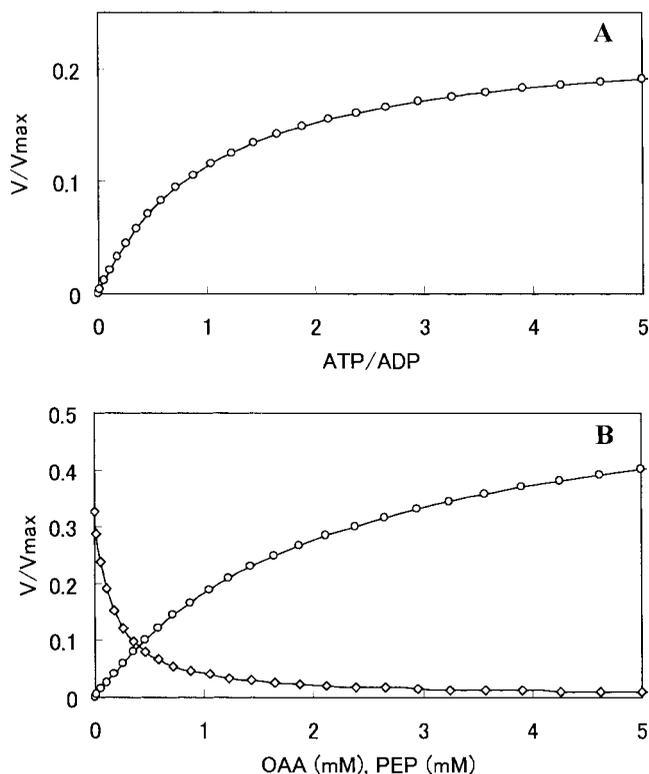
Figure 5. Predicted dependences of the flux through PEP carboxykinase on the ATP/ADP concentration ratio (A) and on the oxaloacetate (○) and PEP (◇) concentrations (B). Both were calculated according to Eq. (16). (A) The concentrations of nonvaried metabolites oxaloacetate and PEP were chosen to be 0.77 mM and 0.17 mM, respectively. (B) The ATP/ADP concentration ratio was chosen to be 1.98. That is, the intracellular metabolite concentrations in *E. coli* W3110 grown at the dilution rate of 0.32 h^{-1} were used for calculations. For abbreviations, see the legend to Figure 1.

intracellular PEP and oxaloacetate pool sizes in wild-type *E. coli* lie in the most sensitive regulatory domain for PEP carboxykinase flux (Table VII). Especially for the changes in PEP concentration within the range of measurement data, the flux varies very sharply.

From the above analysis, it is clear that the in vivo regulation of the PEP carboxykinase flux in *E. coli* occurs mainly by modulation of enzyme activity and by the changes in PEP and oxaloacetate concentration, rather than by ATP/ADP concentration ratio. This regulatory mechanism implies that the reaction catalyzed by gluconeogenic PEP carboxykinase can respond very flexibly to the availability of PEP and oxaloacetate. It is known that PEP is a very important intermediate in *E. coli* metabolism, because it alone directly regulates not only the PTS system but the enzymes phosphofructokinase and pyruvate kinase as well. Due to the activity of PEP carboxykinase, PEP can be generated gluconeogenically from the TCA cycle. It is thus suggested that the reaction catalyzed by PEP carboxykinase in *E. coli* serve to maintain the relative balance between oxaloacetate and PEP pools and drain off excess carbon of the TCA cycle to supply PEP for cellular requirements. Moreover, flux analysis of *pck* deletion mutant indicates that due to abolishment of PEP carboxykinase activity, the

PEP carboxylase cannot solely fulfill the anaplerotic function and the glyoxylate shunt also participates in replenishing the TCA cycle (Fig. 4). Consequently, an important inference from the present study is that the gluconeogenic PEP carboxykinase is not an enzyme that just consumes ATP via the futile cycle without any biological purposes, but plays a key role in anaplerosis and metabolic regulations during the growth of *E. coli* on glucose.

In vivo Regulation of PEP Carboxylation and Glyoxylate Shunt

Significant changes in anaplerotic fluxes were found in response to PEP carboxykinase knockout in *E. coli* (Table V and Fig. 4). Abolishment of PEP carboxykinase activity resulted in a significantly reduced PEP carboxylase flux and the activation of the glyoxylate shunt. Combining the determined in vivo fluxes with the measured data of intracellular metabolite concentrations and specific enzyme activities, the in vivo regulation of PEP carboxylation and glyoxylate shunt in *E. coli* was analyzed.

Gluconeogenic phosphoenolpyruvate carboxylation is generally considered as the sole anaplerotic reaction during growth of *E. coli* on glucose. This is also confirmed by our flux results of wild-type *E. coli* (Fig. 3). However, the in vivo flux through PEP carboxylase decreased sevenfold in the *pck* deletion mutant when compared to wild-type *E. coli* (Fig. 4). In contrast to the in vivo flux, no significant difference in the specific activity of PEP carboxylase was found for the mutant strain (Table VI), indicating that in vivo regulation of anaplerotic PEP carboxylase flux was exerted at the activity level via the changes in metabolite concentrations.

The PEP carboxylase activity in *E. coli* was very low without any activator and acetyl-CoA turned out to be a very potent activator (Table VI). The *pck* deletion mutant exhibited a slightly reduced acetyl-CoA pool size (Table VII), which was consistent with the decrease in PEP carboxylase flux. The sensitivity index for PEP carboxylase flux with respect to intracellular acetyl-CoA concentration, defined as $(\Delta\nu_{ppc}/\Delta[ACoA]) \cdot ([ACoA]/\nu_{ppc})$, was 1.13 within the range of our measured concentrations of acetyl-CoA, which was calculated based on the data of Izui et al. (1981). This finding indicates that the flux reduction of PEP carboxylase in the *pck* deletion mutant may not be caused solely by a change in acetyl-CoA concentration.

Severe inhibition of the PEP carboxylase activity can be caused by L-aspartate and L-malate. Particularly, L-aspartate is a usual inhibitor of the PEP carboxylase from various sources (Kai et al., 1999). However, according to the study of Izui et al. (1981), the PEP carboxylase flux is sensitive to the changes in aspartate and malate pool sizes only if the concentrations of aspartate and malate fall below 1 mM. Since the intracellular aspartate concentration was found to be larger than 2 mM in all cases and almost unchanged in both the wild-type and the *pck* deletion mutant (Table VII), aspartate could probably be ruled out as an

essential inhibitor of PEP carboxylase under in vivo conditions. On the other hand, the measured malate concentrations were less than 0.15 mM in all cases (Table VII). Within this concentration range, the PEP carboxylase flux was very sensitive to alterations of the malate concentration. Furthermore, the intracellular malate concentration was found to be increased in the *pck* deletion mutant when compared to the wild-type strain (Table VII), consistent with the decrease in PEP carboxylase flux. Our results thus suggest that in vivo PEP carboxylation in *E. coli* may be regulated by the intracellular acetyl-CoA and malate rather than by aspartate.

The glyoxylate bypass was found to be activated due to abolishment of PEP carboxykinase activity in the *pck* deletion mutant (Table V and Fig. 4). The regulation of the glyoxylate shunt in *E. coli* has been demonstrated to be the result of reversible phosphorylation of the isocitrate dehydrogenase (ICDH) by Walsh and Koshland (1985). During growth on acetate, a large fraction of ICDH is inactivated to its phosphorylated form. This regulatory mechanism of ICDH might also be present in the *pck* deletion mutant. Consistently, a drastic reduction in the ICDH activity of the mutant was found by our enzyme activity analyses (Table VI). The reversible phosphorylation/inactivation of ICDH is catalyzed by a bifunctional enzyme, ICDH-kinase/phosphatase. As has been pointed out by Holms (1986), the ICDH-kinase/phosphatase is regulated by a number of effectors including oxaloacetate. Oxaloacetate inhibits the IDH-kinase and stimulates the phosphatase. Our study showed that the intracellular oxaloacetate concentration decreased upon *pck* deletion (Table VII), thereby suggesting that a shortage of intracellular oxaloacetate causes the phosphorylation/inactivation of ICDH and the flux through the glyoxylate shunt to replenish the oxaloacetate in the *pck* deletion mutant. Another intermediate, 3-phosphoglycerate, which acts as an important regulatory effector responsible for the phosphorylation of ICDH during growth on acetate (Cronan and LaPorte, 1996), is unlikely to play the same role in the *pck* deletion mutant, because the pool size of 3-phosphoglycerate was found to be approximately identical in both the wild-type strain and the mutant (Table VII).

In *E. coli*, the genes encoding for isocitrate lyase (*aceA*), malate synthase (*aceB*), and ICDH-kinase/phosphatase (*aceK*) form the acetate operon (*aceBAK*). The expression of this operon is induced during growth on acetate or fatty acids but repressed in the presence of glucose. The mechanism by which derepression of the glyoxylate shunt in the *pck* deletion mutant has been achieved is currently unknown. It has been found that the operon is negatively controlled at transcription by IclR, a repressor protein, and release of this repressor is presumably responsible for induction of operon expression during growth on acetate (Cronan and LaPorte, 1996).

Our measurement of metabolite pool sizes found an increase in intracellular isocitrate concentration in the *pck* deletion mutant when compared to the wild-type strain (Table VII). This may be explained by the phosphorylation/ inactivation of ICDH upon *pck* deletion that has a very high affinity for isocitrate (i.e., $K_m = 8$ μM). With the increase in isocitrate concentration, the flux through isocitrate lyase increases dramatically, because the intracellular isocitrate concentration is below the K_m of isocitrate lyase (604 μM). The ICDH is less sensitive to the availability of isocitrate, as ICDH operates largely in the zero-order region (i.e., [ICT] > K_m). Due to this branch point effect, the flux through the glyoxylate bypass is remarkably sensitive to the phosphorylation state of ICDH, and the inactivation of ICDH by phosphorylation and the simultaneous induction of isocitrate lyase activity may thus be sufficient to direct 23% of isocitrate to the glyoxylate shunt in the *pck* deletion mutant.

Metabolic flux responses to PEP carboxykinase knockout in *Corynebacterium glutamicum* have been determined previously (Petersen et al., 2001). The reduced in vivo flux through anaplerotic PEP carboxylase was also found in the PEP carboxykinase-deficient *C. glutamicum*. However, deletion of *pck* in *C. glutamicum* does not lead to the activation of the glyoxylate shunt. This flux difference between *E. coli* and *C. glutamicum* is probably due to the different anaplerotic metabolism. *Corynebacterium glutamicum* possesses two anaplerotic enzymes carboxylating C$_3$ metabolites, PEP carboxylase and pyruvate carboxylase. During the growth of *C. glutamicum* on glucose, pyruvate carboxylase contributes a major fraction to C$_3$ carboxylation (Petersen et al., 2000). Hence, although abolishment of PEP carboxykinase activity in *C. glutamicum* causes a remarkably reduced PEP carboxylase flux, the remaining anaplerotic function can be fulfilled by pyruvate carboxylase. In *E. coli*, however, there is no evidence for the presence of pyruvate carboxylase, and the glyoxylate bypass is activated to participate in anaplerosis upon *pck* deletion.

Significant changes in the intracellular anaplerotic fluxes were observed in response to the PEP carboxykinase knockout in *E. coli* (Figs. 3, 4). However, the pool sizes of the intermediates (i.e., 3-phosphoglycerate, PEP, pyruvate, acetyl-CoA, α-ketoglutarate, aspartate) that are precursors for biosynthesis differed only slightly in the *pck* deletion mutant when compared to the wild-type strain (Table VII). It may thus hypothesized that *E. coli* changes the anaplerotic fluxes for homeostasis of these intermediate concentrations, since the availability of the precursor metabolites has an important impact on the cell growth. Additionally, due to the capability of the *pck* deletion mutant to operate the TCA cycle and the glyoxylate shunt simultaneously, it is very likely that this mutant can grow on high concentration glucose at high yield without producing acetate. A similar metabolic flux pattern has been found in a low acetate producer, *E. coli* BL21, by Noronha et al. (2000), who concluded that the low acetate production is attributed to the activation of the glyoxylate shunt. Acetate accumulation is a common problem of aerobic high cell density *E. coli* cultures for recombinant protein production. Furthermore, the *pck* deletion mutant was found to exhibit a significantly increased biomass yield on glucose when compared to wild-type *E. coli* (Table IV). Hence, based on our findings the

PEP carboxykinase-deficient *E. coli* may be considered as a candidate producer of recombinant proteins.

References

Bergmeyer HU. 1984. Methods of enzymatic analysis, 3rd edition, Vol. 6. Weinheim, Germany: VCH.

Bergmeyer HU. 1985. Methods of enzymatic analysis, 3rd edition, Vol. 7. Weinheim, Germany: VCH.

Canonaco F, Hess TA, Heri S, Wang T, Szyperski T, Sauer U. 2001. Metabolic flux response to phosphoglucose isomerase knock-out *Escherichia coli* and impact of overexpression of the soluble transhydrogenase UdhA. FEMS Microbiol Lett 204:247–252.

Chao YP, Liao JC. 1994. Metabolic responses to substrate futile cycling in *Escherichia coli*. J Biol Chem 269:5122–5126.

Chassagnole C, Noisommit-Rizzi N, Schmid JW, Mauch K, Reuss M. 2002. Dynamic modeling of the central carbon metabolism of *Escherichia coli*. Biotechnol Bioeng 79:53–73.

Cronan JE JR., LaPorte D. 1996. Tricarboxylic acid cycle and glyoxylate bypass. In: Neidhardt FC, Curtiss R, Ingraham JL, Lin ECC, Low KB, Magasanik B, Reznikoff WS, Riley M, Schaechter M, Umbarger HE, eds. *Escherichia coli* and *Salmonella:* Cellular and molecular biology. Washington, DC: ASM Press. p 206–216.

Datsenko KA, Wanner BL. 2000. One-step inactivation of chromosomal genes in *Escherichia coli* K-12 using PCR products. Proc Natl Acad Sci USA 97:6640–6645.

Dauner M, Sauer U. 2001. Stoichiometric growth model for riboflavin-producing Bacillus subtilis. Biotechnol Bioeng 76:132–143.

Dauner M, Bailey JE, Sauer U. 2001a. Metabolic flux analysis with a comprehensive isotopomer model in *Bacillus subtilis*. Biotechnol Bioeng 76:144–156.

Dauner M, Storni T, Sauer U. 2001b. *Bacillus subtilis* metabolism and energetics in carbon-limited and excess-carbon chemostat culture. J Bacteriol 183:7308–7317.

de Koning W, van Dam K. 1992. A method for the determination of changes of glycolytic metabolites in yeast on a subsecond time scale using extraction at neutral pH. Anal Biochem 204:118–123.

Emmerling M, Dauner M, Ponti A, Fiaux J, Hochuli M, Szyperski T, Wuthrich K, Bailey JE, Sauer U. 2002. Metabolic flux responses to pyruvate kinase knockout in *Escherichia coli*. J Bacteriol 184: 152–164.

Flores S, Gosset G, Flores N, de Graaf AA, Bolivar F. 2002. Analysis of carbon metabolism in *Escherichia coli* strains with an inactive phosphotransferase system by ^{13}C labeling and NMR spectroscopy. Metab Eng 4:124–137.

Flores N, Xiao J, Berry A, Bolivar F, Valle F. 1996. Pathway engineering for the production of aromatic compounds in *Escherichia coli*. Nat Biotechnol 14:620–623.

Fraenkel DG. 1996. Glycolysis. In: Neidhardt FC, Curtiss R, Ingraham JL, Lin ECC, Low KB, Magasanik B, Reznikoff WS, Riley M, Schaechter M, Umbarger HE, eds. *Escherichia coli* and *Salmonella:* Cellular and molecular biology. Washington, DC: ASM Press. p 189–198.

Goldberg DM, Ellis G. 1983. Isocitrate dehydrogenase. In: Bergmeyer J,Grassl M, eds. Methods of enzymatic analysis, 3rd edition, Vol. 3. Weinheim, Germany: VCH. p 183–190.

Gombert AK, dos Santos MM, Christensen B, Nielsen J. 2001. Network identification and flux quantification in the central metabolism of *Saccharomyces cerevisiae* under different conditions of glucose repression. J Bacteriol 183:1441–1451.

Holms WH. 1986. The central metabolic pathways of *Escherichia coli:* Relationship between flux and control at a branch point, efficiency of conversion to biomass, and excretion of acetate. Curr Top Cell Regul 28:69–105.

Hua Q, Araki M, Koide Y, Shimizu K. 2001. Effects of glucose, vitamins, and DO concentrations on pyruvate fermentation using *Torulopsis glabrata* IFO 0005 with metabolic flux analysis. Biotechnol Prog 17: 62–68.

Izui K, Taguchi M, Morikawa M, Katsuki H. 1981. Regulation of *Escherichia coli* phosphoenolpyruvate carboxylase by multiple effectors *in vivo*. II. Kinetic studies with a reaction system containing physiological concentrations of ligands. J Biochem 90:1321–1331.

Kai Y, Matsumura H, Inoue T, Terada K, Nagara Y, Yoshinaga T, Kihara A, Tsumura K, Izui K. 1999. Three-dimensional structure of phosphoenolpyruvate carboxylase: A proposed mechanism for allosteric inhibition. Proc Natl Acad Sci USA 96:823–828.

Krebs A, Bridger WA. 1980. The kinetic properties of phosphoenolpyruvate carboxykinase of *Escherichia coli*. Can J Biochem 58:309–318.

Lowry OH, Rosebrough NJ, Farr AJ, Randall RJ. 1951. Protein measurement with the Folin phenol reagent. J Biol Chem 193:265–275.

Maaheimo H, Fiaux J, Cakar ZP, Bailey JE, Sauer U, Szyperski T. 2001. Central carbon metabolism of *Saccharomyces cerevisiae* explored by biosynthetic fractional ^{13}C labeling of common amino acids. Eur J Biochem 268:2464–2479.

Marx A, de Graaf AA, Wiechert W, Eggeling L, Sahm H. 1995. Determination of the fluxes in the central metabolism of *Corynebacterium glutamicum* by nuclear magnetic resonance spectroscopy combined with metabolite balancing. Biotechnol Bioeng 49:111–129.

McFadden BA. 1969. Isocitrate lyase. In: Lowenstein JM, ed. Methods in enzymology, Vol. 13. New York: Academic Press. p 163–170.

Noronha SB, Yeh HJC, Spande TF, Shiloach J. 2000. Investigation of the TCA cycle and the glyoxylate shunt in *Escherichia coli* BL21 and JM109 using ^{13}C-NMR/MS. Biotechnol Bioeng 68:316–327.

Petersen S, de Graaf AA, Eggeling L, Mollney M, Wiechert W, Sahm H. 2000. *In vivo* quantification of parallel and bidirectional fluxes in the anaplerosis of *Corynebacterium glutamicum*. J Biol Chem 275: 35932–35841.

Petersen S, Mack C, de Graaf AA, Riedel C, Eikmanns BJ, Sahm H. 2001. Metabolic consequences of altered phosphoenolpyruvate carboxykinase activity in *Corynebacterium glutamicum* reveal anaplerotic regulation mechanisms *in vivo*. Metab Eng 3:344–361.

Sauer U, Hatzimanikatis V, Bailey JE, Hochuli M, Szyperski T, Wuthrich K. 1997. Metabolic fluxes in riboflavin-producing *Bacillus subtilis*. Nat Biotechnol 15:448–452.

Sauer U, Lasko DR, Fiaux J, Hochuli M, Glaser R, Szyperski T, Wuthrich K, Bailey JE. 1999. Metabolic flux ratio analysis of genetic and environmental modulations of *Escherichia coli* central carbon metabolism. J Bacteriol 181:6679–6688.

Schmidt K, Carlsen M, Nielsen J, Villadsen J. 1997. Modeling isotopomer distributions biochemical networks using isotopomer mapping matrices. Biotechnol Bioeng 55:831–840.

Schmidt K, Norregaard LC, Pedersen B, Meissner A, Duus JO, Nielsen J, Villaden J. 1999. Quantification of intracellular metabolic fluxes from fractional enrichment and ^{13}C-^{13}C coupling constraints on the isotopomer distribution in labeled biomass components. Metab Eng 1: 166–179.

Szyperski T. 1995. Biosynthetically directed fractional ^{13}C-labeling of proteinogenic amino acids. An efficient analytical tool to investigate intermediary metabolism. Eur J Biochem 232:433–448.

Szyperski T. 1998. ^{13}C-NMR, MS and metabolic flux balancing in biotechnological research. Q Rev Biophys 31:41–106.

Szyperski T, Bailey JE, Wuthrich K. 1996. Detecting and dissecting metabolic fluxes using biosynthetic fractional ^{13}C labeling and two-dimensional NMR spectroscopy. Trends Biotechnol 14:453–459.

Vallino JJ, Stephanopoulos G. 1993. Metabolic flux distribution in *Corynebacterium glutamicum* during growth and lysine overproduction. Biotechnol Bioeng 41:633–646.

Varma A, Palsson BO. 1995. Parametric sensitivity of stoichiometric flux balance models applied to wild-type *Escherichia coli* metabolism. Biotechnol Bioeng 45:69–79.

Walsh K, Koshland DE Jr. 1985. Branch point control by the phosphorylation state of isocitrate dehydrogenase. J Biol Chem 260:8430–8437.

Wendisch VF, de Graaf AA, Sahm H, Eikmanns BJ. 2000. Quantitative determination of metabolic fluxes during coutilization of two carbon sources: Comparative analyses with *Corynebacterium glutamicum* during growth on acetate and/or glucose. J Bacteriol 182:3088–3096.

Wiechert W. 2001. ^{13}C metabolic flux analysis. Metab Eng 3:195–206.

Williamson JR, Corkey BE. 1969. Assays of intermediates of the citric acid cycle and related compounds of fluorometric enzyme methods. In: Lowenstein JM, ed. Methods in enzymology, Vol. 13. New York: Academic Press. p 434–513.

Yang C, Hua Q, Shimizu K. 2000. Energetics and carbon metabolism during growth of microalgal cells under photoautotrophic, mixotrophic and cyclic light-autotrophic/dark-heterotrophic conditions. Biochem Eng J 6:87–102.

Yang C., Hua Q, Shimizu K. 2002. Quantitative analysis of intracellular metabolic fluxes using GC-MS and two-dimensional NMR spectroscopy. J Biosci Bioeng 93:78–87.